Nonlinear Stability Analysis of the Classical Nested PI Control of Voltage Sourced Inverters

Monshizadeh, Nima; Mancilla-David, Fernando; Ortega, Romeo; Cisneros, Rafael

Published in:
IEEE Control Systems Letters

DOI:
10.1109/LCSYS.2021.3107747

Publication date:
2022

Nonlinear Stability Analysis of the Classical Nested PI Control of Voltage Sourced Inverters

Nima Monshizadeh, *Member, IEEE*, Fernando Mancilla-David, *Member, IEEE*, Romeo Ortega, *Life Fellow, IEEE*, and Rafael Cisneros

***Abstract*—This note provides the first *nonlinear* analysis of the industry standard "partial decoupling plus nested PI loops" control of voltage sourced inverters. In spite of its enormous popularity, to date only *linearization-based* tools are available to carry out the analysis, which are unable to deal with large-signal stability and fail to provide estimates of the domain of attraction of the desired equilibrium. Instrumental to establish our result is the representation of the closed-loop dynamics in a suitable Lure-like representation, that is, a forward system in closed-loop with a static nonlinearity. The stability analysis is then done by generating an adequate Popov multiplier. Comparison with respect to linearization is discussed together with numerical results demonstrating non-conservativeness of the proposed conditions.**

***Index Terms*—Voltage sourced inverters, Lyapunov analysis, nested PI.**

I. Introduction

GRID–CONNECTED voltage sourced inverters (VSIs) are a central component of many modern electrical generation and distribution facilities. The dynamics of VSIs is described by complicated nonlinear models. Hence, designing control strategies that ensure their suitable operation is a challenging task. Several linear and nonlinear controller design techniques for VSIs have been reported in the literature, including: predictive [1], table-based [2], fuzzy logic [3], repetitive [4], neural networks [5], sliding mode [6] and flatness [7]. To the best of our knowledge, a rigorous nonlinear stability analysis of all these schemes is conspicuous by its absence. Moreover, these controllers have received an, at best, lukewarm reception within the power electronic community, which overwhelmingly prefers the, by-now classical, "partial decoupling plus nested-loop PI" (PD+NLPI) control configuration (in the dq-coordinates). PD+NLPI was first proposed in the 1990' for high power applications in the context of flexible ac transmission systems [8]. Since then, the control has been suggested for several other applications including distributed energy resources [9], photovoltaic power plants [10] and electric vehicles [11].

In the PD+NLPI scheme, a first control action that decouples the current components is implemented. Then, an inner PI loop is wrapped around the current errors, one of whose references is generated via an external PI loop driven by the square of the DC link voltage error [13]—see [12] for details on the controller. The rationale to justify this control configuration relies on the, often reasonable, assumption of time-scale separation between the current and the voltage dynamics. It is widely accepted that, with a *suitable tuning* of the PI gains, the performance of this scheme is satisfactory. The critical commissioning stage of the controller is, invariably, carried out via a *linearization-based* analysis for computing the gains associated to the DC link voltage controller. Consequently, the resulting stability guarantees offer no insights on large-signal stability of the system and do not provide any estimates of the region of attraction.

In spite of its enormous success, to the best of our knowledge, a rigorous nonlinear analysis of the stability of this scheme has not been reported. The main contribution of this letter is to (partially) fill-up this gap with the main motivation of establishing dynamic stability certificates for the VSI system. To this end, we decompose the system in a "Lure-like" form and derive dissipativity-based conditions under which Lyapunov stability of the overall system is guaranteed. Considering this level of generality, however, comes at a price, namely the proposed conditions become difficult to verify in practice despite their theoretically appealing nature. Therefore, we provide numerically efficient Popov-based conditions that ensure existence of quadratic storage functions verifying the former dissipativity property; see [15], [16], for applications of Popov criterion to power systems, and [18], [19] for other attempts in large signal analysis of VSIs. Unlike linearization, our approach can cope with deviations in the operating condition and the constructed Lyapunov functions provide estimates of the region of attraction. We assert the non-conservativeness of our approach through a combined analytical and numerical investigation.

Manuscript received June 2, 2021; revised July 29, 2021; accepted August 12, 2021. Date of publication August 25, 2021; date of current version September 3, 2021. Recommended by Senior Editor C. Prieur. *(Corresponding author: Nima Monshizadeh.)*

Nima Monshizadeh is with the Engineering and Technology Institute, University of Groningen, 9747 AG Groningen, The Netherlands (e-mail: n.monshizadeh@gmail.com).

Fernando Mancilla-David is with the Department of Electrical Engineering, University of Colorado Denver, Denver, CO 80217 USA.

Romeo Ortega and Rafael Cisneros are with the Departamento Académico de Sistemas Digitales, ITAM, Mexico City 01080, Mexico.

Digital Object Identifier 10.1109/LCSYS.2021.3107747

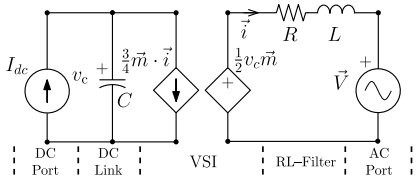

Fig. 1. Equivalent circuit schematic of the VSI system.

II. VSI Model and PD+NLPI Controller

Fig. 1 illustrates the average equivalent circuit of the grid–connected VSI system studied in this letter [12]. The complex variables in the circuit, $\vec{m}$, $\vec{i}$ and $\vec{V}$, correspond to dynamic phasor representations ($\vec{a} = a_d + ja_q$) of the dq components for the corresponding AC quantities. They represent, respectively, the average value of the VSI's modulation index, the current injected into the AC grid, and the grid voltage at the point of interconnection. The VSI is modeled using controlled sources. The AC voltage synthesized by the VSI, $\frac{1}{2}v_c\vec{m}$, is connected to the grid via an *RL* filter, which allows to control the injected current by acting on the modulation index. The scalar variable $v_c > 0$ is the voltage across the DC link capacitor, C, and the current source I_{dc} represents the power source connected to the VSI's DC side. It is noted all quantities on the DC side are scalar, as the operation $\vec{m}\cdot\vec{i}$ corresponds to the dot product. From an active power balance viewpoint, it is observed that the action of the modulation index on the AC side may increase (decrease) the demand of power on the DC side, which, if v_c is kept constant, will have to be drawn from (delivered to) the DC power source. Considering that in a dynamic phasor framework the voltage/current relationship for an inductor is $\vec{v} = L\dot{\vec{i}} + j\omega L\vec{i}$, the dynamics for the circuit of Fig. 1 can be readily established as,

$$L\dot{\vec{i}} = -R\vec{i} - jL\omega\vec{i} + \frac{1}{2}v_c\vec{m} - \vec{V}$$
$$C\dot{v}_c = I_{dc} - \frac{3}{4}\vec{m}\cdot\vec{i}$$

where it is assumed that the overall system (converter and AC grid) is synchronized at the grid frequency ω. The signals V_d, V_q, and ω are assumed to be constant throughout our analysis. In practice, these signals are measured at the point of interconnection with the AC grid. This assumption is customary while studying grid connected VSIs [12] and it is based on the fact that the AC grid is very stiff compared to the VSI. The control objective is to select the modulation index to ensure a desired, assignable equilibrium that is asymptotically stable.

In the PD+NLPI controller a first control of the form $\vec{m} = \frac{2}{v_c}(j\omega L\vec{i} + \vec{V} + \vec{u})$ is implemented, where $\vec{u} := u_1 + ju_2$ is the control signals to be defined. This yields the dynamics

$$L\dot{\vec{i}} = -R\vec{i} + \vec{u} \tag{1a}$$
$$C\dot{v}_c = I_{dc} - \frac{3}{2}\frac{1}{v_c}(\vec{V} + \vec{u})\cdot\vec{i} \tag{1b}$$

which decouples the dynamics in the AC side. To simplify the notation, we write the voltage equation in terms of the signal v_c^2 and define the vector $\mathrm{col}(x_1, x_2, x_3) := \mathrm{col}(i_d, i_q, v_c^2)$. Also, we define the control input $u := \mathrm{col}(u_1, u_2)$ which is generated via

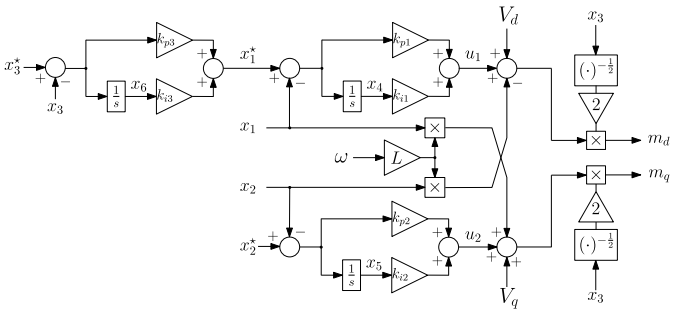

Fig. 2. Block diagram of nested PI control for VSIs.

the nested PI control configuration depicted in Fig. 2, where $x_2^\star$ and $x_3^\star$ are, respectively, the reference for the quadrature current x_2 and the DC voltage squared x_3, which are *fixed* by the designer.

Inspecting the block diagram, the control signals are

$$u_1 = k_{p1}k_{p3}(x_3^\star - x_3) + k_{p1}k_{i3}x_6 - k_{p1}x_1 + k_{i1}x_4 \tag{2a}$$
$$u_2 = k_{p2}(x_2^\star - x_2) + k_{i2}x_5, \tag{2b}$$

where x_4, x_5, x_6 are the state variables of the controllers. By separating (1a) in real and imaginary parts and using the control signal definitions from (2), the state-space closed-loop system in terms of variables x_i becomes,

$$\begin{aligned}
L\dot{x}_1 &= -(R + k_{p1})x_1 + k_{p1}k_{p3}(x_3^\star - x_3) \\
&\quad + k_{p1}k_{i3}x_6 + k_{i1}x_4 \\
L\dot{x}_2 &= -Rx_2 + k_{p2}(x_2^\star - x_2) + k_{i2}x_5 \\
C\dot{x}_3 &= 2I_{dc}\sqrt{x_3} + x_2\big[V_q + k_{p2}(x_2^\star - x_2) + k_{i2}x_5\big] \\
&\quad - 3x_1[V_d + k_{p1}k_{p3}(x_3^\star - x_3) + k_{p1}k_{i3}x_6 - k_{p1}x_1 + k_{i1}x_4] \\
\dot{x}_4 &= k_{p3}(x_3^\star - x_3) + k_{i3}x_6 - x_1 \\
\dot{x}_5 &= x_2^\star - x_2 \\
\dot{x}_6 &= x_3^\star - x_3.
\end{aligned} \tag{3}$$

The objective of this letter is carry-out a *nonlinear* stability analysis of the dynamics of the system (3), and thus providing dynamic stability certificates for the VSI system.

Remark 1: By physical operation constraints, the voltage $v_c > 0$. However, the inverter can, in general, operate in all 4 quadrants in the i_d/i_q plane.

III. Assignable Equilibria and Error Equations

A. Assignable Equilibrium Points

The lemma below parameterizes all the equilibrium points that can be assigned with the controller. To ensure that this set is nonempty we require the following condition.[1]

Assumption 1: The reference values $x_2^\star, x_3^\star > 0$ satisfy

$$V_d^2 - 4R\ell \geq 0, \quad \ell := x_2^\star(V_q + Rx_2^\star) - \frac{2I_{dc}}{3}\sqrt{x_3^\star}. \tag{4}$$

[1]This assumption is necessary for the existence of an equilibrium as the corresponding algebraic equations lead to a quadratic equation whose radial, given by (4), must be nonnegative.

Lemma 1: Fixing the values $x_2^\star$ and $x_3^\star > 0$ of satisfying (4), the set of assignable equilibria of (3) is given by

$$\mathcal{E} = \{x^\star \in \mathbb{R}^6 \mid x_1^\star = \frac{1}{2R}(-V_d \pm \sqrt{V_d^2 - 4R\ell}),$$
$$x_4^\star = \frac{R}{k_{i1}}x_1^\star,\ x_5^\star = \frac{R}{k_{i2}}x_2^\star,\ x_6^\star = \frac{1}{k_{i3}}x_1^\star\}, \tag{5}$$

Proof: The proof follows from straightforward algebraic calculations and is omitted due to lack of space. ∎

B. Error Equations

To shift the equilibrium point to the origin, the change of coordinates $\tilde{x} = x - x^\star$ is introduced. In this error coordinates, we have

$$\begin{aligned}
\dot{\tilde{x}}_1 &= \frac{1}{L}\big[-(R+k_{p1})\tilde{x}_1 - k_{p1}k_{p3}\tilde{x}_3 + k_{p1}k_{i3}\tilde{x}_6 + k_{i1}\tilde{x}_4\big]\\
\dot{\tilde{x}}_2 &= \frac{1}{L}[-(R+k_{p2})\tilde{x}_2 + k_{i2}\tilde{x}_5]\\
\dot{\tilde{x}}_3 &= \frac{2}{C}I_{dc}\sqrt{\tilde{x}_3 + x_3^\star} - \frac{3}{C}(\tilde{x}_2 + x_2^\star)\big[a_2 - k_{p2}\tilde{x}_2 + k_{i2}\tilde{x}_5\big]\\
&\quad - \frac{3}{C}\big[(\tilde{x}_1 + x_1^\star)(a_1 - k_{p1}\tilde{x}_1 - k_{p1}k_{p3}\tilde{x}_3 + k_{i1}\tilde{x}_4 + k_{p1}k_{i3}\tilde{x}_6)\big]\\
\dot{\tilde{x}}_4 &= -k_{p3}\tilde{x}_3 + k_{i3}\tilde{x}_6 - \tilde{x}_1,\quad \dot{\tilde{x}}_5 = -\tilde{x}_2,\quad \dot{\tilde{x}}_6 = -\tilde{x}_3
\end{aligned} \tag{6}$$

where we defined $a_1 := V_d + Rx_1^\star$ and $a_2 := V_q + Rx_2^\star$.

C. Revealing a Cascaded Structure

To begin with the stability analysis task we make two important observations: first, that dynamics of the coordinates $\tilde{x}_2$ and $\tilde{x}_5$ is described by

$$\begin{bmatrix}\dot{\tilde{x}}_2\\ \dot{\tilde{x}}_5\end{bmatrix} = \begin{bmatrix}-\frac{R+k_{p2}}{L} & \frac{k_{i2}}{L}\\ -1 & 0\end{bmatrix}\begin{bmatrix}\tilde{x}_2\\ \tilde{x}_5\end{bmatrix}, \tag{7}$$

which is an LTI system that is *asymptotically stable* for all positive values of k_{p2} and k_{i2}—a choice of sign gains that is always used in practice. Second, that $\tilde{x}_2$ and $\tilde{x}_5$ enter *additively* to the rest of the dynamics, namely to $\dot{\tilde{x}}_3$, as

$$\nu(\tilde{x}_2, \tilde{x}_5) := -\frac{3}{C}(\tilde{x}_2 + x_2^\star)(a_2 - k_{p2}\tilde{x}_2 + k_{i2}\tilde{x}_5) + \frac{3}{C}x_2^\star a_2, \tag{8}$$

where we have included the last term on the right hand side to enforce $\nu(0,0) = 0$. Therefore, this dynamics may be extracted from the rest of the system and their effect treated via cascaded systems arguments. For the sake of brevity we omit the latter part of the analysis and study only the stability of the system assuming, in the sequel, that $\tilde{x}_2 = \tilde{x}_5 = 0$ (see Remark 4).

IV. Absolute Stability Analysis

In this section we carry-out the stability analysis of (6) by isolating a static nonlinearity from the rest of the dynamics and use the techniques in absolute stability theory, notably the Popov criterion [14, Ch. 7.1.2].

A. "Lure-Like" Representation of the System

Note that all nonlinear terms of the system (6) enter into the equation of $\tilde{x}_3$, and the remaining dynamics are linear. Therefore, to analyze the stability of the system it seems reasonable to seek a representation with a static nonlinearity depending only on $\tilde{x}_3$. This is not possible with a standard Lure representation, i.e., with an LTI forward system but can be achieved with a *nonlinear* forward system as follows

$$\dot{z} = \mathcal{A}(z_1)z - Bu \tag{9a}$$
$$\xi = B^\top z = z_4 \tag{9b}$$
$$u = -\phi(\xi) \tag{9c}$$

where $z := \mathrm{col}(\tilde{x}_1, \tilde{x}_4, \tilde{x}_6, \tilde{x}_3)$, $\mathcal{A}(z_1) :=$

$$\begin{bmatrix} I_3 & 0\\ 0 & \frac{3}{C}(z_1 + x_1^\star)\end{bmatrix}\begin{bmatrix} -\frac{1}{L}(R+k_{p1}) & \frac{k_{i1}}{L} & \frac{1}{L}(k_{p1}k_{i3}) & -\frac{k_{p1}k_{p3}}{L}\\ -1 & 0 & k_{i3} & -k_{p3}\\ 0 & 0 & 0 & -1\\ (k_{p1} - \frac{a_1}{z_1 + x_1^\star}) & -k_{i1} & -k_{p1}k_{i3} & k_{p1}k_{p3}\end{bmatrix},$$

$B = \begin{bmatrix}0 & 0 & 0 & 1\end{bmatrix}^\top$ and $\phi : \mathbb{R} \to \mathbb{R}_{\geq 0}$ is given by

$$\phi(\xi) := \frac{2}{C}I_{dc}\sqrt{(\xi + x_3^\star)} - \frac{3}{C}x_1^\star a_1 - \frac{3}{C}x_2^\star a_2.$$

The term $(z_1 + x_1^\star)(= i_d)$ is factored out for convenience of the presentation. Notice that this term, that may cross to zero, cancels in the matrix $\mathcal{A}(z_1)$, hence there is no division by it in the dynamics. Also, it is easy to see that the solutions of (9) are well-defined and exist for all time as long as $(z_4 + x_3^\star)(= v_c) > 0$, which is consistent with the operating regime of the inverter—see Remark 1. Note that the negative signs in (9a) and (9c) are added to write the system as a *negative* feedback interconnection.

We observe that $\phi(\xi) = 0$ if and only if $\xi = 0$. The lemma below identifies a sector condition for the static nonlinearity $\phi(\cdot)$, that will be instrumental for our analysis.

Lemma 2: Fix a constant $c \in (0, x_3^\star]$ and define the neighborhood

$$\Omega_c := \{z \in \mathbb{R}^4 \mid \|z\| < c\}.$$

The static nonlinearity $\phi(z_4)$ satisfies in Ω_c the sector condition

$$0 \leq \gamma(c)z_4\phi(z_4) \leq z_4^2, \qquad \gamma(c) := \frac{C\sqrt{x_3^\star - c}}{I_{dc}}. \tag{10}$$

Proof: Using the mean value theorem and $\phi(0) = 0$, we have

$$z_4\phi(z_4) = z_4^2\frac{d\phi}{dz_4}(\hat{z}_4) = z_4^2\left(\frac{I_{dc}}{C\sqrt{\hat{z}_4 + x_3^\star}}\right),$$

where $\hat{z}_4$ belongs to the line connecting the points 0 and z_4. Since $|z_4| < c \leq x_3^*$, the expression on the right hand side of the above equalities is well-defined and attain its supremum at $\hat{z}_4 = -c$. The latter results in the upper bound in (10) and completes the proof. ∎

B. Popov-Based Lyapunov Analysis

Before proceeding with the analysis, and inspired by the Popov criterion [14], the following is assumed:

Assumption 2: There exists a positive-definite storage function $V : \mathbb{R}^4 \to \mathbb{R}_{\geq 0}$ and scalars $\rho \geq 0$, $\epsilon > 0$ such that the system (9a), (9b) satisfies the dissipation inequality

$$\dot{V}(z) \leq -\epsilon|z|^2 + \gamma(c)u^2 + u(\xi + \rho\dot{\xi}) \tag{11}$$

for all $z \in \Omega_c$ and $u \in \mathcal{U}$, where $\mathcal{U}$ is the set of all inputs keeping z in Ω_c.

Proposition 1: Let Assumption 2 hold. Then, the origin is an asymptotically stable equilibrium of (9). In particular, we have $\dot{W}(z) \leq -\epsilon|z|^2$, where

$$W(z) \coloneqq V(z) + \rho \int_0^{z_4} \phi(\xi)d\xi. \tag{12}$$

Proof: Under Assumption 2, we have

$$\dot{V} = -\epsilon|z|^2 + \gamma(c)\phi^2(\xi) - \phi(\xi)(\xi + \rho\dot{\xi})$$

Therefore, bearing in mind that $\xi = z_4$,

$$\begin{aligned}\dot{W} &= -\epsilon|z|^2 + \gamma(c)\phi^2(z_4) - \phi(z_4)(z_4 + \rho\dot{z}_4) + \rho\phi(z_4)\dot{z}_4 \\ &= -\epsilon|z|^2 + \gamma(c)\phi^2(z_4) - \phi(z_4)z_4\end{aligned}$$

We claim that $\dot{W} \leq -\epsilon|z|^2$ by verifying

$$\gamma(c)\phi(z_4)^2 - \phi(z_4)z_4 \leq 0. \tag{13}$$

The inequality above is trivially satisfied for $z_4 = 0$. For $z_4 \neq 0$, we have

$$\gamma(c)\phi^2(z_4) - \phi(z_4)z_4 = \phi^2(z_4)z_4^2\left(\frac{\gamma(c)}{z_4^2} - \frac{1}{z_4\phi(z_4)}\right) \leq 0,$$

where the inequality follows from (10). The proof is completed noting that $W(z)$ is positive definite. ∎

Remark 2: From (10) we see that the term $\gamma(c)$ is inversely proportional to the slope of the static nonlinearity $\phi(\cdot)$, and positively contributes to the feasibility of the dissipation inequality (11). If the input-output map $u \to \xi$ is (strictly) passive, then no restriction will be imposed on the slope of the nonlinearity by choosing $\rho = 0$ and allowing $\gamma(c)$ to be arbitrary small. As this map deviates from a passive one, a tighter constraint should be imposed on the slope of nonlinearity in order to satisfy the dissipation inequality.

C. Verifying Assumption 2

Assumption 2 has been used in the preceding Lyapunov stability results. However, the condition (11) can be difficult to verify in practice. Therefore, we provide a sufficient condition for (11), which can be conveniently checked.

Lemma 3: Suppose that there exists a positive definite matrix $P \in \mathbb{R}^{4\times 4}$ and scalars $\epsilon_1 > 0$ and $c_1 \in (0, x_3^\star]$ such that

$$\begin{aligned}&z^\top(\mathcal{A}^\top(0)P + P\mathcal{A}(0) + \epsilon_1 P)z + 2z^\top PBu \\ &\quad\leq \gamma(c_1)u^2 + u(\xi + \rho\dot{\xi}).\end{aligned} \tag{14}$$

Then, Assumption 2 holds for any c satisfying

$$0 < c < \min\left(c_1, \frac{\epsilon_1\lambda_{\min}(P)}{2\|\delta\|\|P\|}\right), \tag{15}$$

where $\delta \coloneqq \frac{3}{C}\begin{bmatrix}k_{p1} & -k_{i1} & -k_{p1}k_{i3} & k_{p1}k_{p3}\end{bmatrix}$.

Proof: Let $\Delta(z_1) \coloneqq \mathcal{A}(z_1) - \mathcal{A}(0)$. Clearly, the first three rows of Δ are zero vectors, and its forth row is given by $z_1\delta$. Now, by taking the quadratic storage function $V(z) = z^\top Pz$ and computing its time derivate along the solutions of the nonlinear system (9), we obtain

$$\dot{V}(z) = z^\top(\mathcal{A}^\top(0)P + P\mathcal{A}(0))z + 2z^\top P\Delta(z_1)z + 2z^\top PBu.$$

By using (14), we find that

$$\dot{V}(z) \leq +2z^\top P\Delta(z_1)z - \epsilon_1 z^T Pz + \gamma(c_1)u^2 + u(\xi + \rho\dot{\xi}).$$

Observe that

$$\begin{aligned}z^\top P\Delta(z_1)z &\leq \|\Delta(z_1)\|\|P\|\|z\|^2 \\ &= |z_1|\|\delta\|\|P\|\|z\|^2 < c\|\delta\|\|P\|\|z\|^2,\end{aligned}$$

where the last inequality follows because $z \in \Omega_c$.

Then, we have

$$\begin{aligned}\dot{V}(z) \leq &-(\epsilon_1\lambda_{\min}(P) - 2c\|\delta\|\|P\|)\|z\|^2 \\ &+ \gamma(c_1)u^2 + u(\xi + \rho\dot{\xi}).\end{aligned}$$

Clearly, for any c satisfying (15), the scalar

$$\epsilon \coloneqq \epsilon_1\lambda_{\min}(P) - 2c\|\delta\|\|P\| > 0.$$

The proof is completed noting that $\gamma(c)$ is a monotonically decreasing function of c, and thus $\gamma(c_1)u^2 \leq \gamma(c)u^2$. ∎

Remark 3: The idea behind Lemma 3 is to borrow the quadratic storage function from the (linear) system (9) with $\mathcal{A}(z_1)$ replaced by $\mathcal{A}(0)$, and leverage it to establish the dissipativity inequality (11). The condition (14) can be efficiently checked as will be discussed in the next subsection.

D. Tuning Guidelines

The control parameters can be selected such that the condition (14) in Lemma 3 is satisfied. This condition can be checked both in frequency-domain and time-domain. In particular, let $G(s)$ denote the transfer function from u to ξ in (9) with $\mathcal{A}(z_1)$ replaced by $\mathcal{A}(0)$, i.e.,

$$G(s) \coloneqq -B^\top(sI_4 - \mathcal{A}(0))^{-1}B. \tag{16}$$

Then, the condition (14) in *frequency-domain* is translated to the perturbed transfer function $H(s) \coloneqq (1 + \rho s)G(s) + \gamma(c_1)$ being strictly positive real [14]. A typical way to verify this property is to plot $G(j\omega)$ in the axes $\mathfrak{Re}(G(j\omega))$, $\omega\mathfrak{Im}(G(j\omega)$, with ω as a parameter—that is, the so-called (Popov plot). Then $H(s)$ is strictly positive real if the plot lies to the right of the line that intercepts the point $-\gamma(c_1)$ with a slope ρ^{-1}. Alternatively, the strict positive real condition can be verified by writing a minimal realization of $H(s)$ and check the LMI conditions of the Kalman–Yakubovich-Popov lemma [14]. Note that the right hand side of (15) is not needed in practice, as one can start with a initial choice of c and keep decreasing it till the aforementioned Popov plot or the LMI condition is satisfied.

Remark 4: To carry out the stability analysis of the *full system* (6), that is, including the term $\nu(\tilde{x}_2, \tilde{x}_5)$ given in (8), we can proceed as follows. First, we impose the following constraint on the storage function $V(z)$ satisfying Assumption 2:

$$\alpha_1|z|^2 \leq V(z) \leq \alpha_2|z|^2$$

for some positive scalars α_1 and α_2—this condition is trivially satisfied for the quadratic storage function in Lemma 3. Then it is easy to see that $W(z)$ in Proposition 1 satisfies a similar constraint in Ω_c for some positive scalars $\bar{\alpha}_1, \bar{\alpha}_2$. Hence, the equilibrium of (9) becomes locally *exponentially* stable, which noting the underlying cascade structure results in local exponential stability of the equilibrium of (6).

E. On the Non-Conservativeness of the Popov Condition

Unlike linearization, a nonlinear Lyapunov analysis allows for deviations from the operating point of the system, which in turn provides insights to nonlinear stability. This advantage, however, often brings some conservatism in the design compared to linearization which only asks for stability with possibly an arbitrary small region of attraction. Next, we argue the nonconservativeness of our Lyapunov results with respect to linearization.

Linearizing (9) around the origin yields,

$$\dot{z} = \left(\mathcal{A}(0) + \frac{1}{\gamma(0)} BB^\top\right) z \tag{17}$$

where $\gamma(0) = \frac{C\sqrt{x_3^\star}}{I_{dc}}$. This results in the following condition:

Lemma 4: The origin is an asymptotically stable equilibrium of the full system (6) if the matrix $\mathcal{A}(0) + \frac{1}{\gamma(0)} BB^\top$ is Hurwitz. This equilibrium is unstable if the state matrix has an eigenvalue with a positive real part.

Proof: The proof follows noting that linearization of (6) amounts to the cascaded interconnection of the linear system (17) with (7). ∎

Let $A_{\text{lin}} \coloneqq \mathcal{A}(0) + \frac{1}{\gamma(0)} BB^\top$ denote the state matrix in (17). Consider the auxiliary transfer function

$$G_{\text{lin}}(s) \coloneqq -B^\top (sI_4 - A_{\text{lin}})^{-1} B.$$

Clearly, if $G_{\text{lin}}(s)$ has any poles on the right half plane, then the matrix A_{lin} has an eigenvalue on the open right half plane, and thus the equilibrium of the nonlinear system is *unstable*. Conversely, under mild stabilizability/detectability conditions, asymptotic stability of the equilibrium can be deduced from that of the transfer function $G_{\text{lin}}(s)$. We now use the Sherman-Morrison formula to rewrite G_{lin}

$$\begin{aligned} G_{\text{lin}}(s) = &-B^\top \left(sI - \mathcal{A}(0) - \frac{1}{\gamma(0)} BB^\top\right)^{-1} B \\ &- B^\top (sI - \mathcal{A}(0))^{-1} B \\ &- \frac{\frac{1}{\gamma(0)} B^\top (sI - \mathcal{A}(0))^{-1} BB^\top (sI - \mathcal{A}(0))^{-1} B}{1 - \frac{1}{\gamma(0)} B^\top (sI - \mathcal{A}(0))^{-1} B}, \end{aligned}$$

which by straightforward calculations yields

$$G_{\text{lin}}(s) = \frac{G(s)}{1 + \frac{1}{\gamma(0)} G(s)}, \tag{18}$$

with $G(s)$ given by (16). Suppose that the transfer function $G(s)$ is minimum phase, which holds for all practically relevant ranges of the physical parameters of the VSI. Then, based on (18) and the Nyquist criterion, the equilibrium is unstable if the Nyquist contour of $G(j\omega)$ encircles the point $(-\gamma(0), 0)$. Now, compare this with the Popov stability condition stated earlier, which asks for the Popov plot of $G(j\omega)$ to lie to the right of a line (with a positive slope) that intercepts the point $(-\gamma(c), 0)$. Note that the value of $\gamma(c)$ tends to $\gamma(0)$ as c and thus the estimates of the region of attraction gets smaller. Our numerical investigation suggests that encirclement of the point $(-\gamma(0), 0)$ in the Nyquist diagram of $G(j\omega)$ coincides with not being able to draw a line passing through $(-\gamma(0), 0)$ which lies to the left of the Popov plot of $G(j\omega)$. The latter suggests non-conservativeness of the Popov condition in our case. The details of this numerical study are provided next.

TABLE I
SIMULATION PARAMETERS

Parameter	Symbol	Value
DC current	I_{dc}	125 A
DC capacitance	C	5000 μF
Filter inductance	L	100 μH
Filter resistance	R	20 mΩ
AC voltage	V_d	187.8 V
AC voltage	V_q	0 V
AC frequency	ω	376.9 rad/s
DC voltage reference	$\sqrt{x_3^\star}$	400 V
AC current reference	$x_2^\star$	0 A

V. A NUMERICAL STUDY

For our numerical study, we select a 50 kVA, 6 kHz VSI that transfers power between a DC port rated at 400 V and a 230 V, 60 Hz three–phase AC grid. Numerical values for the physical and control parameters are in Table I.

The tuning process of the PI controller gains is usually approached relying on the temporal decoupling between the outer loop (DC voltage control) and the two inner loops (AC current control). It is noted from (1) that both AC currents feature identical dynamics, and if the PI controller gains are chosen as $k_{p1} = k_{p2} = L/\tau$ and $k_{i1} = k_{i2} = R/\tau$ then the transfer functions $x_1/x_1^\star$ and $x_2/x_2^\star$ become $1/(1+\tau s)$, which are stable and feature a speed response determined by τ. In the results that follow we present plots parametrized in terms of τ, which is selected by the designer. To simplify the comparison, and to isolate the role of τ, we fix the gains $k_{p3} = -0.0086$ and $k_{i3} = -1.4532$.[2] We increase the value of τ from 4ms to 5ms, and plot the resulting Nyquist diagrams of $G(s)$ given by (16). Following the discussion after (18), the equilibrium of the system becomes unstable as soon as the Nyquist plot encircles the point $(-\gamma(0), 0) = (-0.016, 0)$. As shown in Fig. 3, this corresponds to the marginal stability threshold of $\tau = 4.53$ ms. Next, we repeat the numerical experiment with the Popov plot in place of the Nyquist diagram. See Fig. 4. Interestingly, the stability certificate provided by the Popov test is valid as long as τ does not exceed the threshold 4.53 ms. This suggests that the proposed Lyapunov analysis is not conservative. Note that the Popov condition is based on Lyapunov analysis whose advantages over linearization are well-known. In particular, the bounded level sets of the Lyapunov function can be used to obtain estimates of the region of attraction (see [14, Ch. 4.1.]).

[2]These values are such that the current control loop is much faster than that of the voltage. We note that one can also explore stability using the Nyquist or the Popov plot over the parameter space given by (τ, k_{p3}, k_{i3}).

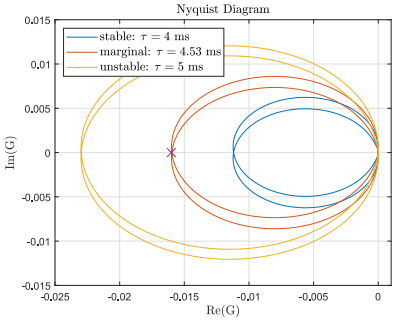

Fig. 3. Nyquist diagram for three values of τ. The point $(-\gamma(0), 0)$ is shown with the symbol $\times$.

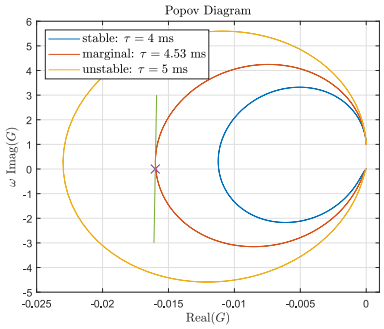

Fig. 4. Popov diagram for three values of τ. The point $(-\gamma(0), 0)$ is shown with the symbol $\times$.

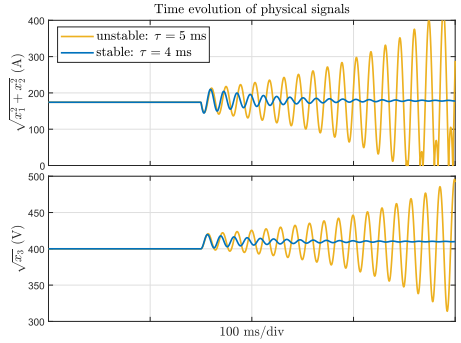

Fig. 5. Time evolution of the DC voltage (bottom plot) and AC current magnitude (top plot). A 10 V step like change (400 V to 410 V) in the DC voltage reference is applied at 150 ms.

The results above have also been validated through detailed simulations, including a three-phase model of the VSI, *abc* to/from *dq* domain transformations, and frequency reading through a phase locked loop. For illustration, we provide the results for a stable and unstable operation, corresponding to $\tau = 4$ ms and $\tau = 5$ ms, respectively. We chose to display the time evolution of the physical signals, i.e., the DC voltage and magnitude of the AC current, for a 10V step like change in the DC voltage reference (Fig. 5).

VI. Concluding Remarks

The disposing of a complete theoretical analysis of the current engineering practice gives the user additional confidence in the design and provides useful guidelines in the difficult task of commissioning the controller. This important task has not been addressed in the control literature—which is instead devoted to proposing "new" controllers. This work aimed to alleviate this situation concentrating on a practically important problem of control of power inverters. The main results are Popov-based conditions under which Lyapunov stability of the controlled power inverters is guaranteed. Assessing performance metrics beyond stability constitutes the main direction for future research.

References

[1] M. G. Judewicz, S. A. Gonzalez, J. R. Fischer, J. F. Martínez, and D. O. Carrica, "Inverter-side current control of grid-connected voltage source inverters with LCL filter based on generalized predictive control," *IEEE Trans. Emerg. Sel. Topics Power Electron.*, vol. 6, no. 4, pp. 1732–1743, Dec. 2018.

[2] H. A. Hamed, A. F. Abdou, S. Acharya, M. S. El. Moursi, and E. E. ELKholy, "A novel dynamic switching table based direct power control strategy for grid connected converters," *IEEE Trans. Energy Convers.*, vol. 33, no. 3, pp. 1086–1097, Sep. 2018.

[3] M. A. Hannan, Z. A. Ghani, A. Mohamed, and M. N. Uddin, "Realtime testing of a fuzzy-logic-controller-based grid-connected photovoltaic inverter system," *IEEE Trans. Ind. Appl.*, vol. 51, no. 6, pp. 4775–4784, Nov./Dec. 2015.

[4] D. Chen, J. Zhang, and Z. Qian, "An improved repetitive control scheme for grid-connected inverter with frequency-adaptive capability," *IEEE Trans. Ind. Electron.*, vol. 60, no. 2, pp. 814–823, Feb. 2013.

[5] X. Fu and S. Li, "Control of single-phase grid-connected converters with LCL filters using recurrent neural network and conventional control methods," *IEEE Trans. Power Electron.*, vol. 31, no. 7, pp. 5354–5364, Jul. 2016.

[6] Z. Li, C. Zang, P. Zeng, H. Yu, S. Li, and J. Bian, "Control of a grid-forming inverter based on sliding-mode and mixed $H_2 - H_\infty$ control," *IEEE Trans. Ind. Electron.*, vol. 64, no. 5, pp. 3862–3872, May 2017.

[7] H. Sira-Ramirez and R. Silva-Ortigoza, *Control Design Techniques in Power Electronics Devices* (Communications and Control Engineering). Berlin, Germany: Springer, 2006.

[8] C. Schauder and H. Mehta, "Vector analysis and control of advanced static VAR compensators," *IEE Proc. Gener. Transm. Distrib.*, vol. 140, no. 4, pp. 299–306, 1993.

[9] F. Blaabjerg, R. Teodorescu, M. Liserre, and A. V. Timbus, "Overview of control and grid synchronization for distributed power generation systems," *IEEE Trans. Ind. Electron.*, vol. 53, no. 5, pp. 1398–1409, Oct. 2006.

[10] M. Carrasco and F. Mancilla-David, "Maximum power point tracking algorithms for single-stage photovoltaic power plants under time-varying reactive power injection," *Solar Energy*, vol. 132, pp. 321–331, Jul. 2016.

[11] A. Arancibia, K. Strunz, and F. Mancilla-David, "A unified single- and three-phase control for grid connected electric vehicles," *IEEE Trans. Smart Grid*, vol. 4, no. 4, pp. 1780–1790, Dec. 2013.

[12] A. Yazdani and R. Iravani, *Voltage-Sourced Converters in Power Systems*. Oxford, U.K.: Wiley-IEEE Press, 2010.

[13] M. K. Mishra and K. Karthikeyan, "A fast-acting DC-link voltage controller for three-phase DSTATCOM to compensate AC and DC loads," *IEEE Trans. Power Del.*, vol. 24, no. 4, pp. 2291–2299, Oct. 2009.

[14] H. K. Khalil, *Nonlinear Systems*, 3rd ed. Upper Saddle River, NJ, USA: Prentice-Hall, 2001.

[15] F. Andrade, K. Kampouropoulos, L. Romeral, J. C. Vasquez, and J. M. Guerrero, "Study of large-signal stability of an inverter-based generator using a Lyapunov function," in *Proc. Annu. Conf. IEEE Ind. Electron. Soc.*, 2014, pp. 1840–1846.

[16] N. Monshizadeh and I. Lestas, "Secant and Popov-like conditions in power network stability," *Automatica*, vol. 101, pp. 258–268, Mar. 2019.

[17] M. Kabalan, P. Singh, and D. Niebur, "A design and optimization tool for inverter-based microgrids using large-signal nonlinear analysis," *IEEE Trans. Smart Grid*, vol. 10, no. 4, pp. 4566–4576, Jul. 2019.

[18] M. Kabalan, P. Singh, and D. Niebur, "Nonlinear Lyapunov stability analysis of seven models of a DC/AC droop controlled inverter connected to an infinite bus," *IEEE Trans. Smart Grid*, vol. 10, no. 1, pp. 772–781, Jan. 2019.

[19] B. Shakerighadi, E. Ebrahimzadeh, F. Blaabjerg, and C. L. Bak, "Large-signal stability modeling for the grid-connected VSC based on the Lyapunov method," *Energies*, vol. 11, no. 10, pp. 1–16, 2018.